
DocKylin: A Large Multimodal Model for Visual Document Understanding with Efficient Visual Slimming

Jiaxin Zhang^{1,*} Wentao Yang^{1,*} Songxuan Lai² Zecheng Xie^{2,†} Lianwen Jin^{1,†}
¹South China University of Technology ²Huawei Cloud

Abstract

Current multimodal large language models (MLLMs) face significant challenges in visual document understanding (VDU) tasks due to the high resolution, dense text, and complex layouts typical of document images. These characteristics demand a high level of detail perception ability from MLLMs. While increasing input resolution improves detail perception, it also leads to longer sequences of visual tokens, increasing computational costs and straining the models' ability to handle long contexts. To address these challenges, we introduce DocKylin, a document-centric MLLM that performs visual content slimming at both the pixel and token levels, thereby reducing token sequence length in VDU scenarios. DocKylin utilizes an Adaptive Pixel Slimming (APS) preprocessing module to perform pixel-level slimming, increasing the proportion of informative pixels. Moreover, DocKylin incorporates a novel Dynamic Token Slimming (DTS) module to conduct token-level slimming, filtering essential tokens and removing others to create a compressed, adaptive visual sequence. Experiments demonstrate DocKylin's promising performance across various VDU benchmarks. Notably, both the proposed APS and DTS are parameter-free, facilitating easy integration into existing MLLMs, and our experiments indicate their potential for broader applications.

1 Introduction

With the substantial growth in data and model sizes, as well as alignment with human preferences, current Large Language Models (LLMs) [45, 65, 63, 2, 62, 73] have demonstrated remarkable capabilities in reasoning, common sense understanding, expertise in specialized knowledge, zero/few-shot learning, and instruction following, shedding light on the potential for Artificial General Intelligence. Multimodal Large Language Models (MLLMs) aim to enhance these powerful LLMs by endowing them with multimodal capabilities, enabling the integration of diverse modalities beyond text alone.

Although there has been significant progress in the development of MLLMs, their performance in visual document understanding (VDU) tasks remains suboptimal [36, 78]. A primary reason for this is their support for input resolutions of only up to 448x448, which is inadequate for high-resolution, fine-grained document images. Numerous efforts [76, 37, 29, 70, 3, 74, 32, 72] have recently been made to increase the input resolution to address this limitation and achieved notable improvements. However, these efforts still face several challenges: **1)** Increasing the resolution also escalates the redundant regions within documents, which results in an increased number of redundant visual tokens, complicating the task for LLMs to identify the correct answers. **2)** Some methods [29, 70, 72, 3] employ a fixed rectangular resolution, which can lead to text distortion given the typically large aspect ratios of document images. Moreover, scaling smaller images to larger ones

*Equal Contribution. † Corresponding Author. This work was conducted during Jiaxin Zhang and Wentao Yang's internship at Huawei Cloud. Emails: xiezecheng1@huawei.com, eelwj@scut.edu.cn

results in inefficiencies. 3) To manage the extended sequences of visual tokens resulting from high resolution, most methods [29, 76, 37, 3] employ a fixed compression ratio or extract a predetermined number of tokens. While this approach may be suitable for natural scene images, it is less effective for document scenarios where content density varies significantly. For example, images of scientific papers are information-dense, whereas images of identification cards are comparatively sparse.

To tackle these challenges, we propose a series of solutions. Firstly, we propose a parameter-free Adaptive Pixel Slimming (APS) preprocessing technique that utilizes gradient information to identify and eliminate redundant regions within document images, thereby reducing the proportion of redundant pixels and enhancing computational efficiency. Secondly, we adopt a more flexible image encoding strategy by capping the maximum number of pixels instead of fixing resolutions. This allows for variable resolutions and aspect ratios. Our lightweight Swin encoder [38] processes high-resolution document images holistically, ensuring feature coherence. Thirdly, we propose a Dynamic Token Slimming (DTS) method based on k-means clustering [39], which is also parameter-free. DTS filters useful tokens from a vast pool of visual tokens, obtaining visual sequences with reduced and dynamic lengths. Incorporating these innovations, we developed our DocKylin, which demonstrates superior performance across multiple VDU benchmarks. Ablation studies further confirm the effectiveness of some of these designs and highlight their potential applicability to other MLLMs or scenarios.

2 Related Works

2.1 Text-centric MLLMs

Text is crucial for understanding images, but the ability of existing MLLMs in this regard is generally subpar [36, 51, 61]. Therefore, there has been a surge of recent work studying how to enhance the perception, recognition, and understanding abilities of text images in MLLMs. Some approaches [58, 23] leverage additional Optical Character Recognition (OCR) engines to recognize text in images and input it into MLLMs. Others [29, 37, 3, 12, 13, 74, 70] enhance the fine-grained perceptual capabilities of MLLMs by maintaining the high resolution of the input images. This includes strategies such as splitting the image into small pieces to accommodate the ViT’s requirement for fixed and small-size inputs and utilizing visual encoders that are more suitable for text images. Authors of [14, 69] explore learning text grounding for MLLMs, while [16, 60] investigate the use of more superior and larger scale instruction data to boost performance. Although these efforts have significantly improved the performance of MLLMs on text-centric tasks, there is still substantial room for improvement.

2.2 Visual Token Compression in MLLMs

Maintaining high-resolution input images is a straightforward and effective method to enhance the performance of MLLMs on text images. However, increased resolutions inevitably lead to a longer sequence of visual tokens. There are various methods for compressing the length of visual sequences in current MLLMs. One of the earlier and commonly used approaches [11, 27, 1] involves utilizing a group of learnable query tokens to extract information in a cross-attention manner. Another method [7, 76] involves concatenating adjacent tokens along the channel dimension to reduce sequence length. Additionally, convolutional neural networks (CNNs) have also been proven effective for visual token compression [6, 16]. However, all these methods either extract tokens of a fixed length or compress them at a fixed ratio. This approach is unsuited for document images, where the content density can vary significantly. A token sequence that is too short or a compression ratio that is too high can result in an inadequate representation of some document images. Conversely, longer token sequences or lower compression rates can reduce computational efficiency.

Recent studies [5] have shown that the optimal length of visual token sequences varies for each sample. Consequently, some recent approaches have explored the adaptive compression of visual sequences. Most of these methods [34, 49, 8, 31] dynamically discard nonessential tokens using attention scores between visual tokens or between visual tokens and class tokens. However, considering the differences between text and natural objects with complete semantics, this paradigm may not be suitable for text images. For text-centric images, HRVDA[72] employs text position annotations to train a separate visual token filtering network, which requires introducing additional parameters training procedures. Compared to the methods above, we explore alternative dynamic compression schemes specifically

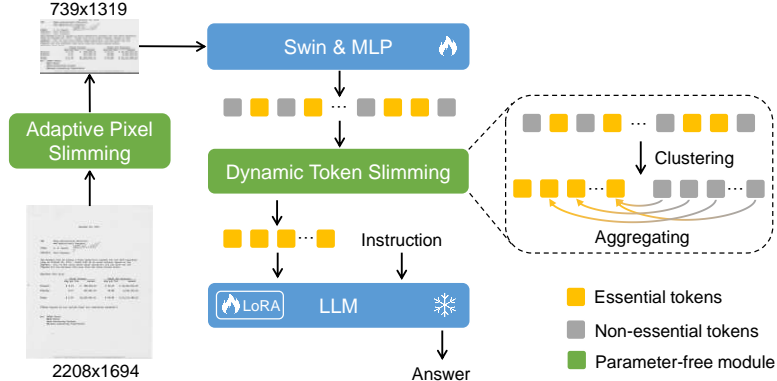


Figure 1: The overall architecture of our DocKylin model.

for document images, which include pixel-level redundancy removal and unsupervised clustering for filtering out nonessential tokens.

3 Methodology

As illustrated in Fig. 1, similar to many multimodal large language models (MLLMs), our architecture also incorporates an image encoder, an MLP layer that aligns the visual modality to the language modality, and a LLM. Building on this framework, DocKylin includes the following enhancements: Images are preprocessed by the Adaptive Pixel Slimming module before being fed to the image encoder, which removes redundant regions and reduces resolution while increasing the proportion of informative pixels. The visual tokens obtained by the visual encoder and MLP layer are handled by our Dynamic Token Slimming (DTS) module to remove nonessential tokens to enhance both performance and efficiency. We provide a detailed description of these improvements in the following.

3.1 Adaptive Pixel Slimming

Perceiving textual information in images typically requires maintaining a high resolution of input, especially for text-rich document images. This poses significant challenges for current resource-intensive MLLMs. To address this issue, existing methods employ strategies such as dividing the images into patches for processing [37, 74], employing visual encoders that support high resolution [70], leveraging OCR results as additional inputs [58, 23], or applying compression transformations to the images beforehand [13].

Here, we propose a novel approach called Adaptive Pixel Slimming (APS) to efficiently reduce the resolution of document images, which is orthogonal to the approaches mentioned above. APS is based on the observation that, as illustrated in Fig. 2, while document images usually exhibit high resolution, they commonly contain a significant proportion of redundant regions. These regions not only increase the computational burden on the visual encoder but may also pose challenges [37, 72] to the reasoning capabilities of the LLMs by the increased redundant visual tokens. APS is thus designed to identify and remove these regions. Specifically, as shown in Fig. 2, during the gradient extraction stage, we utilize the Sobel operator to extract the gradient map I_G from the original image I_S . Regions with low gradient values are considered smooth and devoid of significant information. Therefore, in the redundant region determination stage, we identify the redundant regions in the horizontal and vertical directions by locating areas with consistently low gradient values. For instance, to identify redundant regions in the image’s horizontal direction: if the sum of gradient values for a specific row is below a predefined threshold, we classify that row as redundant. A sequence of contiguous redundant rows constitutes a redundant region in the horizontal direction. The computation for the vertical direction follows a similar procedure. The final image can be obtained by removing the identified redundant rows and columns. For more details on the algorithm and parameter settings, please refer to the Appendix.

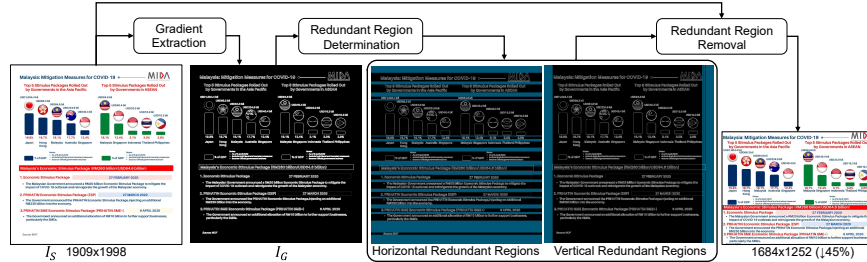


Figure 2: Schematic representation of the Adaptive Pixel Slimming module. It effectively reduces the resolution of document images by removing redundant regions.

Table 1: Changes in image resolution before and after the application of Adaptive Pixel Slimming, as well as the resulting reduction in pixel count.

Datasets	Adaptive Pixel Slimming	Avg. Resolution	Reduction
DocVQA	✗	1748 × 2088	-
	✓	1531 × 1524	36.0%
InfoVQA	✗	1181 × 2541	-
	✓	1120 × 2193	18.1%

Table 1 presents the reduction in image resolution after applying our APS module, which demonstrates that APS significantly decreases the resolution of images. Some visual results are available in the Appendix. It is worth noting that APS is primarily designed for document images, where redundant regions are commonly distinctly defined. In contrast, elements in natural scene images tend to be more complex, making it challenging to identify extensive redundant regions. Consequently, APS generally has a limited impact on natural scene tasks. In the subsequent experimental section of our paper, we demonstrate that the application of APS consistently improves performance on multiple document image benchmarks without adversely affecting tasks involving natural scenes.

3.2 More Flexible Image Encoding

Most existing MLLMs [29] utilize a fixed rectangular resolution, such as 224×224 or 336×336 . This approach distorts the original aspect ratio of the images, leading to text deformation and inefficiencies when upscaling images smaller than the preset resolution. While some methods [74, 76] allow for more flexible aspect ratios and resolutions, they often employ a patch-based processing strategy. Such a strategy may be suitable for natural scene images where the continuity and context of visual elements are less critical. However, it is less effective for document images [37] that contain dense text. Segmenting such images can disrupt the textual content, severing lines of text or splitting words and sentences across different patches. This discontinuity can impair the ability to accurately recognize and interpret textual information essential for effective document image understanding.

We employ a more flexible approach that can accommodate varying resolutions and aspect ratios without the need for image patching. Specifically, for an image obtained by APS with the size of $H \times W$, we set a maximum allowable number of pixels, MAX_SIZE. If the product of H and W is less than MAX_SIZE, the image will not be resized. Otherwise, a scaling factor $r = \text{Int}(\sqrt{\frac{\text{MAX_SIZE}}{H \times W}})$ is calculated, and then the image is resized to $rH \times rW$. Here $\text{Int}()$ denotes the floor function to ensure that the resulting image does not exceed the maximum allowable pixels. One advantage of setting a maximum number of pixels rather than fixed dimensions is the ability to support more varied resolutions and preserve the original aspect ratio. Additionally, this manner avoids the loss of image details due to resolution reduction as much as possible without increasing computational resource consumption. For example, if we set the maximum pixels number MAX_SIZE as 960×960 , we can accommodate an input resolution of 1280×720 without alteration. In contrast, a fixed-dimension strategy would require resizing the image to 960×960 , resulting in a 25% compression of the long side. Both strategies consume comparable computational resources since the number of visual tokens remains consistent.

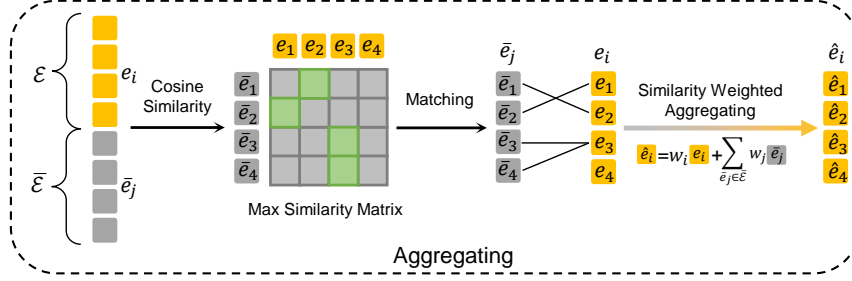


Figure 3: Schematic diagram of the proposed Similarity Weighted Aggregation module. The aggregation module aggregates nonessential tokens into essential tokens through similarity weighted summation.

Although ViT pre-trained with CLIP [48] demonstrates impressive generalization capabilities for natural scene images, they perform suboptimally on dense document images [28]. Furthermore, their self-attention mechanism, which has a computational complexity that scales quadratically with image resolution, makes it challenging to support high-resolution inputs. Consequently, we opt to use the more efficient Swin Transformer [38] as our visual encoder, which has been pre-trained on full-text recognition tasks [22]. It enables us to process entire images as single inputs.

3.3 Dynamic Token Slimming

Although the APS module has been effective in removing some redundant regions, it is limited to processing entire rows or columns and is ineffective for more complex scenarios. In contrast, our Dynamic Token Slimming (DTS) method offers a more flexible approach to eliminate redundant visual content at the token level. The design of the DTS is based on the premise that a well-trained visual encoder should be capable of effectively distinguishing between essential and nonessential regions within an image, with the features corresponding to different regions exhibiting sufficient discriminative properties. We propose to separate these two types of tokens directly through clustering and then aggregate nonessential tokens into essential tokens. We next detail the proposed DTS, which comprises two main processes: Dual-center K-Means Clustering and Similarity Weighted Aggregation.

Dual-center K-Means Clustering. To distinguish tokens into essential and nonessential types without introducing additional parameters, we apply K-Means clustering [39] with two centers to the output sequence from the visual encoder, as illustrated in Fig 1. However, after obtaining the two clusters, it is unclear which cluster contains the essential tokens and which contains the non-essential tokens. Drawing on findings from [37], nonessential tokens typically lack uniqueness and are often similar to other tokens. Therefore, we identify potential nonessential tokens by evaluating the similarity of each visual token with all other ones. The cluster with fewer of these nonessential tokens is determined to be the one containing the essential tokens. For more implementation details, please refer to Algorithm 1.

Algorithm 1 Dual-center K-Means Clustering

Require:

visual tokens from Image Encoder: $V = \mathbb{R}^{L \times D}$
 visual tokens from MLP Layer: $V' = \text{MLP}(V) \in \mathbb{R}^{L \times D'}$
 CMX (calculate min similarity)
 $R = 50$

- 1: cluster1, cluster2 = $K\text{-means}(V, \text{center_num} = 2)$
 - 2: max_similarities = []
 - 3: **for** token in V' :
 - 4: max_similarities.append(CMX(token, other tokens in V'))
 - 5: top-R_similar_tokens = select_top(V' , max_similarities, R)
 - 6: num1 = num_of_same_tokens(top-R_similar_tokens, cluster1)
 - 7: num2 = num_of_same_tokens(top-R_similar_tokens, cluster2)
 - 8: **if** num1 > num2:
 - 9: essential_tokens = cluster2
 - 10: nonessential_tokens = cluster1
 - 11: **else:**
 - 12: essential_tokens = cluster1
 - 13: nonessential_tokens = cluster2
 - 14: **return** essential_tokens, nonessential_tokens
-

Similarity Weighted Aggregation. After obtaining essential and nonessential tokens, how to handle the nonessential tokens becomes a crucial issue. Inspired by [24, 30, 71], to mitigate potential clustering errors and prevent information loss, we do not discard the nonessential tokens outright. Instead, we aggregate them into the essential tokens to minimize the potential loss of effective

information while enhancing the model’s processing efficiency. As illustrated in Fig. 3, for each nonessential token from the clustering step, we find the most similar essential token. Each essential token may correspond to zero or multiple nonessential tokens. If an essential token has corresponding nonessential tokens, we perform a similarity weighted summation of these tokens to obtain an aggregated token.

Specifically, after determining the set of essential tokens $\mathcal{E} = \{e_1, e_2, e_3, \dots, e_N\}$ and the set of nonessential tokens $\bar{\mathcal{E}} = \{\bar{e}_1, \bar{e}_2, \bar{e}_3, \dots, \bar{e}_N\}$, we aggregate nonessential tokens \bar{e}_j into essential tokens e_i by similarity weighted summation:

$$\hat{e}_i = w_i e_i + \sum_{\bar{e}_j \in \bar{\mathcal{E}}} w_j \bar{e}_j, \quad (1)$$

where w_i and w_j are the weight for the i -th essential and j -th nonessential token, and \hat{e}_i is the aggregated token. We use the similarity between e_i and \bar{e}_j to determine w_i and w_j . Specifically, we first define the similarity matrix between essential tokens and nonessential tokens:

$$c_{i,j} = \frac{e_i^T \bar{e}_j}{\|e_i\| \|\bar{e}_j\|}. \quad (2)$$

Next, we obtain a mask matrix to ensure that each nonessential token is aggregated only with the most similar essential token:

$$m_{i,j} = \begin{cases} 1, & i = \arg \max_{\bar{e}_j \in \bar{\mathcal{E}}} c_{i,j}, \\ 0, & \text{otherwise,} \end{cases} \quad (3)$$

Finally, we can obtain aggregating weight w_j and w_i by:

$$w_j = \frac{\exp(c_{i,j}) m_{i,j}}{\sum_{\bar{e}_j \in \bar{\mathcal{E}}} \exp(c_{i,j}) m_{i,j} + e} \quad (4)$$

and

$$w_i = \frac{e}{\sum_{\bar{e}_j \in \bar{\mathcal{E}}} \exp(c_{i,j}) m_{i,j} + e}. \quad (5)$$

The pseudo-code for the specific implementation can be found in Algorithm 3 in the appendix.

4 Experiments

4.1 Implementation Details

Our model underwent two training stages: pre-training and instruction tuning. Training data used in each phase are listed in Table 2. During the pre-training stage, we trained only the visual encoder and the MLP, keeping the LLM parameters fixed. In this phase, the model learns to perform full-text recognition on document images and convert charts and tables into markdown formats [16]. The goal is to enable the visual encoder to comprehend document content and align the visual features with the language space through the MLP.

During the pre-training phase, the model was trained for 450,000 iterations with a batch size of 8. The learning rate decayed from $1e-4$ to $1e-5$ using cosine annealing, which took approximately 40 A800 GPU-days. In the instruction tuning phase, the model underwent 300,000 iterations with the same batch size and learning rate as in the pre-training phase. This phase further consumed approximately 24 A800 GPU-days. Our Adaptive Pixel Slimming method is employed in both phases, while the Dynamic Token Slimming (DTS) is used only during the instruction tuning phase. The maximum allowed number of pixels, MAX_SIZE, is set to 1728×1728 . We initialize our visual encoder with Donut-Swin (0.07B) [22], pre-trained on the reading texts task, and use Qwen-7B-Chat [2] as our LLM.

Table 2: Datasets used in pre-training and instruction tuning phase.

Stage	Datasets
Pre-training	CASIA-HWDB [33], CCpdf [66], ChartQA [40], DeepForm [57], DocVQA [42], DVQA [20], FigureQA [21], InfoVQA [41], KLC [54], OCRVQA [44], PlotQA [43], PubTabNet [79], RVL-CDIP [15], SCUT-HCCDoc [77], SynthDog [22], TAT-QA [80], VisualMRC [59], WildReceipt [56]
Instruction tuning	ChartQA [40], DeepForm [57], DocILE [52], DocVQA [42], DVQA [20], InfoVQA [41], InsuranceQA [55], KLC [54], OCR-TROSD[64], TAT-QA [80], VisualMRC [59], WildReceipt [56], WTQ [46]

Table 3: Quantitative accuracy (%) comparison of DocKylin with existing general-purpose MLLMs on document image benchmarks. Accuracy proposed in [78] is adopted as the metric for all benchmarks.

Methods	Visual Encoder (Params.)	DocVQA ^{val}	InfoVQA ^{val}	ChartQA	FUNSD	SROIE	POIE
mPLUG-Owl [75]	CLIP-L (0.3B)	7.4	20.0	7.9	0.2	0.1	0.3
InstructBLIP [11]	CLIP-G (2B)	4.5	16.4	5.3	0.2	0.6	1.0
LLaVA1.5 [35]	CLIP-L (0.3B)	8.5	14.7	9.3	0.2	1.7	2.5
Qwen-VL [3]	CLIP-G (2B)	48.1	23.9	53.4	23.9	34.5	20.6
Monkey [29]	CLIP-G (2B)	<u>50.1</u>	25.8	<u>54.0</u>	<u>24.1</u>	<u>41.9</u>	19.9
InternVL [9]	IVI ^T (6B)	28.7	23.6	45.6	6.5	26.4	25.9
InterLM-XComposer2 [12]	CLIP-L (0.3B)	39.7	<u>28.6</u>	51.6	15.3	34.2	49.3
DocKylin (ours)	Swin (0.07B)	65.1	34.8	58.7	25.5	49.5	<u>36.1</u>

Table 4: Quantitative comparison of DocKylin with existing text-centric MLLMs on document-oriented benchmarks. The metrics used for each benchmark are consistent with those proposed in the original papers.

Methods	Visual Encoder (Params.)	DocVQA ^{test}	InfoVQA ^{test}	ChartQA	VisualMRC	DeepForm	WTQ
Donut [22]	Swin (0.07B)	67.5	11.6	41.8	93.9	61.6	18.8
Pix2Struct[26]	-	76.6	40.0	58.6	-	-	-
mPLUG-Doc [75]	CLIP-L (0.3B)	62.2	38.2	57.4	188.8	42.6	26.9
UReader [74]	CLIP-L (0.3B)	65.4	42.2	65.7	221.7	49.5	29.4
DocPeida [13]	Swin (0.1B)	47.1	15.2	46.9	-	-	-
HRVDA [72]	Swin	72.1	43.5	67.6	211.5	63.2	31.2
Vary [70]	ViTDet-B & CLIP-L (0.4B)	76.3	-	66.1	-	-	-
TextMonkey [37]	CLIP-G (2B)	71.5	-	65.5	-	61.6	30.6
TextHawk [76]	SigLIP-SO (0.4B)	<u>76.4</u>	50.6	66.6	-	-	34.7
LayoutLLM-LLaMA2 [17]	LayoutLMv3-L (0.3B)	74.3	-	-	-	-	-
DocKylin (ours)	Swin (0.07B)	77.3	<u>46.6</u>	<u>66.8</u>	319.9	64.2	<u>32.4</u>

4.2 Comparisons on VDU Benchmarks

We first compare our model with several existing general-purpose multimodal large language models (MLLMs). As these models sometimes tend to provide detailed responses, following [78], we adopt accuracy as our metric: a response is considered correct if it contains the complete answer. The results, as shown in Table 3, demonstrate that DocKylin achieves a significant advantage over the competing models. This highlights that VDU tasks remain challenging for current general-purpose MLLMs. Note that descriptions of all these benchmarks are included in the Appendix.

We also compare our model with several current text-centric MLLMs. The results, presented in Table 4, use the same metrics as those employed in the original benchmarks. Detailed descriptions of the specific metrics used for each benchmark can be found in the Appendix. Our method demonstrates advantages over these text-centric MLLMs, achieving leading performance across multiple benchmarks. Notably, our visual encoder is more lightweight than those used by the compared methods.

Some visual results from DocKylin on these benchmarks are presented in Fig. 4. The first row shows the results of redundant regions detected by APS, with corresponding text explaining the resulting reduction in resolution. The second row displays the nonessential tokens removed by DTS, with accompanying text illustrating its effect on compressing the visual sequence. These results demonstrate their effectiveness in accurately retaining important regions while significantly reducing the resolution and the length of the visual sequence.

To further demonstrate the superiority of our method, we compared it with other parameter-free visual token compression methods, using LLaVA1.5 [35] as our baseline model (without retraining). The results in Table 5 indicate that our APS and DTS achieve performance improvements with shorter sequence lengths compared to the baseline model, significantly outperforming existing SOTA compression methods. It is worth noting that these results are achieved without retraining. Typically, after retraining, models can better adapt to the new mode of compressed token sequences, leading to further performance improvements [49, 8].

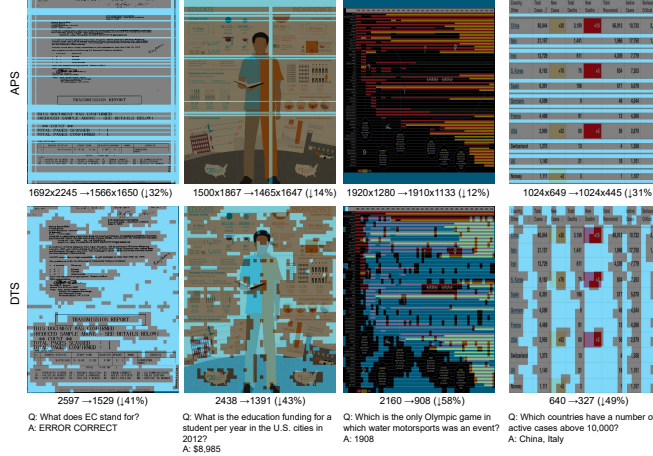


Figure 4: Visualization from DocKylin. The redundant pixels and nonessential tokens identified by Adaptive Pixel Slimming and Dynamic Token Slimming are highlighted in light blue.

Table 5: Comparisons with current SOTA parameter-free visual token compression methods. Accuracy proposed in [78] is adopted as the metric for all benchmarks.

Model	Compression	Adaptive	DocVQA ^{val}		InfoVQA ^{val}		SROIE	
			Avg. len	Acc ↑	Avg. len	Acc ↑	Avg. len	Acc ↑
	-	-	576	8.5	576	14.7	576	1.7
	Random	✗	300	5.4	300	14.3	300	0.5
	Random	✗	200	4.2	200	14.2	200	0
LLaVA1.5 [35]	FastV (K=2, R=50%) [8]	✗	306	8.4	306	14.4	306	2.0
	PruMerge [49]	✓	123	5.3	123	13.8	121	0.4
	PruMerge+ [49]	✓	232	5.2	233	14.0	229	0.3
	APS+DTS (ours)	✓	298	9.7	270	14.7	296	3.1

4.3 Ablation Studies and Potential Broader Applications

We validate the effectiveness of APS and DTS on DocKylin and give the results in Table 6. Note that, settings without DTS in Table 6 refer to retraining a new model from scratch without employing DTS in the instruction tuning phase, rather than simply removing DTS from the already trained DocKylin model. The results demonstrate that both APS and DTS effectively reduce token sequence length and enhance computational efficiency, while also improving performance. This aligns with findings from previous studies [37], which suggest that excessively long sequences due to high resolution may degrade performance. This degradation likely occurs because the visual sequences contain too many redundant tokens, placing greater demands on the model’s ability to handle long contexts and making the learning more challenging. Notably, the APS and DTS methods can also be used online during the training phase to accelerate training. Specifically, applying the DTS method during the instruction tuning phase can reduce training time by approximately 15%.

Since APS is a parameter-free method that requires no additional training or modification of model architecture, it is easily applicable to other MLLMs to enhance their performance on high-resolution document images. To demonstrate its effectiveness, we apply APS to various existing MLLM models (employing it before the image processing module of these models). As shown in Table 7 of our

Table 6: Ablation studies on DocKylin regarding Adaptive Pixel Slimming and Dynamic Token Slimming. The latency and training time are normalized to the results in the first row. Accuracy proposed in [78] is adopted as the metric for all benchmarks.

APS	DTS	Avg. Token Len	Training Time	DocVQA ^{val}	
				Acc.	Latency
✗	✗	2770	1	63.1	1
✓	✗	2198	0.97	64.5	0.81
✓	✓	1250	0.86	65.1	0.61

Table 7: The enhancement brought to other MLLMs by Adaptive Pixel Slimming. **Relative improvements** are highlighted in bold. Accuracy proposed in [78] is adopted as the metric for all benchmarks.

Methods	Resolution	TextVQA	DocVQA ^{val}	InfoVQA ^{val}	SROIE	FUNSD
LLaVA1.5 [35]	336×336	38.7	8.5	14.7	1.7	0.2
LLaVA1.5 [35] + APS	336×336	40.2 (+ 4.1%)	10.7 (+ 27.4%)	14.7 (+ 0%)	3.7 (+ 118%)	0.92 (+ 360%)
Qwen-VL [3]	448×448	62.1	48.1	23.9	34.5	20.6
Qwen-VL [3] + APS	448×448	62.4 (+ 0.4%)	51.2 (+ 6.4%)	24.7 (+ 4.1%)	40.0 (+ 15.9%)	24.3 (+ 17.9%)
Monkey [29]	896×896	64.3	50.1	25.8	41.9	24.1
Monkey [29] + APS	896×896	65.2 (+ 1.4%)	56.3 (+ 12.4%)	27.5 (+ 6.6%)	47.0 (+ 12.2%)	27.3 (+ 13.3%)

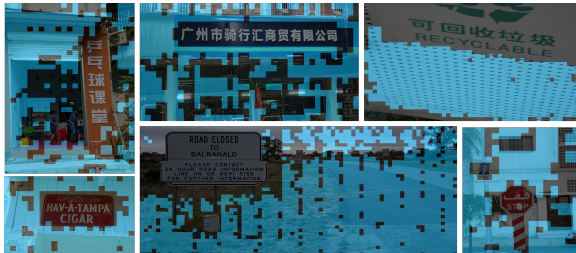


Figure 5: Effects of applying DTS to natural scene images.

experimental results, APS consistently improves document image tasks across a range of MLLMs with different resolutions. Additionally, results on TextVQA demonstrate that APS does not lead to performance degradation in tasks involving scene images.

The redundant regions in document images are often simple, such as plain backgrounds, distinguishing these regions is relatively easy. This raises the question of whether DTS’s effectiveness is due to this simplicity. Although this paper primarily explores VDU tasks, we are also interested in the generalizability of DTS. Therefore, we conducted some experiments on natural scene images. Specifically, we retrained a scene text image full-text recognition model using some open-source scene text data [10, 53, 50, 68], performing only the first pre-training phase. We then applied DTS to the trained model and tested it on the TextVQA dataset. Some visual results are shown in Fig. 5. It can be seen that DTS is effective in distinguishing nonessential regions even in the complex backgrounds of natural scene images.

5 Limitations

While DocKylin exhibits outstanding performance in visual document understanding (VDU) tasks, it currently lacks versatility for more general tasks, such as question answering and captioning in natural scenes. This limitation primarily stems from our current image encoder, which has not undergone extensive image-text pair pre-training and also possesses insufficient parameter capacity. Future work could explore scaling up the Swin Transformer and conducting pre-training similar to that of the current CLIP ViT. Alternatively, a dual-encoder approach [32, 70] could be employed, where a flexible, lightweight Swin Transformer is specifically used for extracting fine textual details within images, while a larger-capacity ViT model is utilized for capturing more general content. The combined image features from both encoders could then be integrated into the LLM.

6 Conclusions

To address the issues of high input resolution and excessively long token sequences in current MLLMs when counters with VDU tasks, we propose the DocKylin model. It includes a parameter-free Adaptive Pixel Slimming (APS) preprocessing module that removes redundant regions from document images, effectively reducing their resolution. The model employs a flexible image encoding approach to adapt to the varying resolutions and aspect ratios of document image scenarios. Moreover, we propose a parameter-free token compression method, Dynamic Token Slimming (DTS), which clusters and selects essential tokens from a long visual sequence and employs aggregation to avoid potential information loss.

Experiments demonstrate that DocKylin achieves leading performance across multiple VDU benchmarks. APS and DTS effectively shorten the length of visual tokens, enhancing both computational efficiency and model performance. Additionally, we have validated the potential of applying these methods to other MLLMs or other scenarios beyond document images.

References

- [1] Jean-Baptiste Alayrac, Jeff Donahue, Pauline Luc, Antoine Miech, Iain Barr, Yana Hasson, Karel Lenc, Arthur Mensch, Katherine Millican, Malcolm Reynolds, et al. Flamingo: a visual language model for few-shot learning. *Advances in neural information processing systems*, 35:23716–23736, 2022. [2](#)
- [2] Jinze Bai, Shuai Bai, Yunfei Chu, Zeyu Cui, Kai Dang, Xiaodong Deng, Yang Fan, Wenbin Ge, Yu Han, Fei Huang, et al. Qwen technical report. *arXiv preprint arXiv:2309.16609*, 2023. [1](#), [6](#)
- [3] Jinze Bai, Shuai Bai, Shusheng Yang, Shijie Wang, Sinan Tan, Peng Wang, Junyang Lin, Chang Zhou, and Jingren Zhou. Qwen-vl: A frontier large vision-language model with versatile abilities. *arXiv preprint arXiv:2308.12966*, 2023. [1](#), [2](#), [7](#), [9](#)
- [4] Ali Furkan Biten, Ruben Tito, Andres Mafla, Lluís Gomez, Marçal Rusinol, Minesh Mathew, CV Jawahar, Ernest Valveny, and Dimosthenis Karatzas. Icdar 2019 competition on scene text visual question answering. In *2019 International Conference on Document Analysis and Recognition (ICDAR)*, pages 1563–1570. IEEE, 2019. [16](#)
- [5] Mu Cai, Jianwei Yang, Jianfeng Gao, and Yong Jae Lee. Matryoshka multimodal models. *arXiv preprint arXiv:2405.17430*, 2024. [2](#)
- [6] Junbum Cha, Wooyoung Kang, Jonghwan Mun, and Byungseok Roh. Honeybee: Locality-enhanced projector for multimodal llm. *arXiv preprint arXiv:2312.06742*, 2023. [2](#)
- [7] Jun Chen, Deyao Zhu, Xiaoqian Shen, Xiang Li, Zechun Liu, Pengchuan Zhang, Raghuraman Krishnamoorthi, Vikas Chandra, Yonyang Xiong, and Mohamed Elhoseiny. Minigt-v2: large language model as a unified interface for vision-language multi-task learning. *arXiv preprint arXiv:2310.09478*, 2023. [2](#)
- [8] Liang Chen, Haozhe Zhao, Tianyu Liu, Shuai Bai, Junyang Lin, Chang Zhou, and Baobao Chang. An image is worth 1/2 tokens after layer 2: Plug-and-play inference acceleration for large vision-language models. *arXiv preprint arXiv:2403.06764*, 2024. [2](#), [7](#), [8](#)
- [9] Zhe Chen, Jiannan Wu, Wenhai Wang, Weijie Su, Guo Chen, Sen Xing, Zhong Muyan, Qinglong Zhang, Xizhou Zhu, Lewei Lu, et al. Internvl: Scaling up vision foundation models and aligning for generic visual-linguistic tasks. *arXiv preprint arXiv:2312.14238*, 2023. [7](#)
- [10] Chee Kheng Ch’ng and Chee Seng Chan. Total-text: A comprehensive dataset for scene text detection and recognition. In *2017 14th IAPR international conference on document analysis and recognition (ICDAR)*, volume 1, pages 935–942. IEEE, 2017. [9](#)
- [11] Wenliang Dai, Junnan Li, Dongxu Li, Anthony Meng Huat Tiong, Junqi Zhao, Weisheng Wang, Boyang Li, Pascale N Fung, and Steven Hoi. Instructblip: Towards general-purpose vision-language models with instruction tuning. *Advances in Neural Information Processing Systems*, 36, 2024. [2](#), [7](#)
- [12] Xiaoyi Dong, Pan Zhang, Yuhang Zang, Yuhang Cao, Bin Wang, Linke Ouyang, Songyang Zhang, Haodong Duan, Wenwei Zhang, Yining Li, et al. Internlm-xcomposer2-4khd: A pioneering large vision-language model handling resolutions from 336 pixels to 4k hd. *arXiv preprint arXiv:2404.06512*, 2024. [2](#), [7](#)
- [13] Hao Feng, Qi Liu, Hao Liu, Wengang Zhou, Houqiang Li, and Can Huang. Docpedia: Unleashing the power of large multimodal model in the frequency domain for versatile document understanding. *arXiv preprint arXiv:2311.11810*, 2023. [2](#), [3](#), [7](#)
- [14] Hao Feng, Zijian Wang, Jingqun Tang, Jinghui Lu, Wengang Zhou, Houqiang Li, and Can Huang. Unidoc: A universal large multimodal model for simultaneous text detection, recognition, spotting and understanding. *arXiv preprint arXiv:2308.11592*, 2023. [2](#)

- [15] Adam W Harley, Alex Ufkes, and Konstantinos G Derpanis. Evaluation of deep convolutional nets for document image classification and retrieval. In *2015 13th International Conference on Document Analysis and Recognition (ICDAR)*, pages 991–995. IEEE, 2015. 6
- [16] Anwen Hu, Haiyang Xu, Jiabo Ye, Ming Yan, Liang Zhang, Bo Zhang, Chen Li, Ji Zhang, Qin Jin, Fei Huang, et al. mplug-docowl 1.5: Unified structure learning for ocr-free document understanding. *arXiv preprint arXiv:2403.12895*, 2024. 2, 6
- [17] Yupan Huang, Tengchao Lv, Lei Cui, Yutong Lu, and Furu Wei. Layoutlmv3: Pre-training for document ai with unified text and image masking. In *Proceedings of the 30th ACM International Conference on Multimedia*, pages 4083–4091, 2022. 7
- [18] Zheng Huang, Kai Chen, Jianhua He, Xiang Bai, Dimosthenis Karatzas, Shijian Lu, and CV Jawahar. Icdar2019 competition on scanned receipt ocr and information extraction. In *2019 International Conference on Document Analysis and Recognition (ICDAR)*, pages 1516–1520. IEEE, 2019. 16
- [19] Guillaume Jaume, Hazim Kemal Ekenel, and Jean-Philippe Thiran. Funsd: A dataset for form understanding in noisy scanned documents. In *2019 International Conference on Document Analysis and Recognition Workshops (ICDARW)*, volume 2, pages 1–6. IEEE, 2019. 16
- [20] Kushal Kafle, Brian Price, Scott Cohen, and Christopher Kanan. Dvqa: Understanding data visualizations via question answering. In *Proceedings of the IEEE conference on computer vision and pattern recognition*, pages 5648–5656, 2018. 6
- [21] Samira Ebrahimi Kahou, Vincent Michalski, Adam Atkinson, Ákos Kádár, Adam Trischler, and Yoshua Bengio. Figureqa: An annotated figure dataset for visual reasoning. *arXiv preprint arXiv:1710.07300*, 2017. 6
- [22] Geewook Kim, Teakgyu Hong, Moonbin Yim, JeongYeon Nam, Jinyoung Park, Jinyeong Yim, Wonseok Hwang, Sangdoon Yun, Dongyoon Han, and Seunghyun Park. Ocr-free document understanding transformer. In *European Conference on Computer Vision*, pages 498–517. Springer, 2022. 5, 6, 7
- [23] Geewook Kim, Hodong Lee, Daehee Kim, Haeji Jung, Sanghee Park, Yoonsik Kim, Sangdoon Yun, Taeho Kil, Bado Lee, and Seunghyun Park. Visually-situated natural language understanding with contrastive reading model and frozen large language models. In *The 2023 Conference on Empirical Methods in Natural Language Processing*, 2023. 2, 3
- [24] Zhenglun Kong, Peiyan Dong, Xiaolong Ma, Xin Meng, Wei Niu, Mengshu Sun, Xuan Shen, Geng Yuan, Bin Ren, Hao Tang, et al. Spvit: Enabling faster vision transformers via latency-aware soft token pruning. In *European conference on computer vision*, pages 620–640. Springer, 2022. 5
- [25] Jianfeng Kuang, Wei Hua, Dingkang Liang, Mingkun Yang, Deqiang Jiang, Bo Ren, and Xiang Bai. Visual information extraction in the wild: practical dataset and end-to-end solution. In *International Conference on Document Analysis and Recognition*, pages 36–53. Springer, 2023. 16
- [26] Kenton Lee, Mandar Joshi, Iulia Raluca Turc, Hexiang Hu, Fangyu Liu, Julian Martin Eisenschlos, Urvashi Khandelwal, Peter Shaw, Ming-Wei Chang, and Kristina Toutanova. Pix2struct: Screenshot parsing as pretraining for visual language understanding. In *International Conference on Machine Learning*, pages 18893–18912. PMLR, 2023. 7
- [27] Junnan Li, Dongxu Li, Silvio Savarese, and Steven Hoi. Blip-2: Bootstrapping language-image pre-training with frozen image encoders and large language models. In *International conference on machine learning*, pages 19730–19742. PMLR, 2023. 2
- [28] Xin Li, Yunfei Wu, Xinghua Jiang, Zhihao Guo, Mingming Gong, Haoyu Cao, Yinsong Liu, Deqiang Jiang, and Xing Sun. Enhancing visual document understanding with contrastive learning in large visual-language models. *arXiv preprint arXiv:2402.19014*, 2024. 5

- [29] Zhang Li, Biao Yang, Qiang Liu, Zhiyin Ma, Shuo Zhang, Jingxu Yang, Yabo Sun, Yuliang Liu, and Xiang Bai. Monkey: Image resolution and text label are important things for large multi-modal models. *arXiv preprint arXiv:2311.06607*, 2023. 1, 2, 4, 7, 9
- [30] Youwei Liang, GE Chongjian, Zhan Tong, Yibing Song, Jue Wang, and Pengtao Xie. Evit: Expediting vision transformers via token reorganizations. In *International Conference on Learning Representations*, 2021. 5
- [31] Zhihang Lin, Mingbao Lin, Luxi Lin, and Rongrong Ji. Boosting multimodal large language models with visual tokens withdrawal for rapid inference. *arXiv preprint arXiv:2405.05803*, 2024. 2
- [32] Ziyi Lin, Chris Liu, Renrui Zhang, Peng Gao, Longtian Qiu, Han Xiao, Han Qiu, Chen Lin, Wenqi Shao, Keqin Chen, et al. Sphinx: The joint mixing of weights, tasks, and visual embeddings for multi-modal large language models. *arXiv preprint arXiv:2311.07575*, 2023. 1, 9
- [33] Cheng-Lin Liu, Fei Yin, Da-Han Wang, and Qiu-Feng Wang. Casia online and offline chinese handwriting databases. In *2011 international conference on document analysis and recognition*, pages 37–41. IEEE, 2011. 6
- [34] Haogeng Liu, Quanzeng You, Xiaotian Han, Yongfei Liu, Huaibo Huang, Ran He, and Hongxia Yang. Visual anchors are strong information aggregators for multimodal large language model. *arXiv preprint arXiv:2405.17815*, 2024. 2
- [35] Haotian Liu, Chunyuan Li, Yuheng Li, and Yong Jae Lee. Improved baselines with visual instruction tuning. *arXiv preprint arXiv:2310.03744*, 2023. 7, 8, 9
- [36] Yuliang Liu, Zhang Li, Hongliang Li, Wenwen Yu, Mingxin Huang, Dezhi Peng, Mingyu Liu, Mingrui Chen, Chunyuan Li, Lianwen Jin, et al. On the hidden mystery of ocr in large multimodal models. *arXiv preprint arXiv:2305.07895*, 2023. 1, 2
- [37] Yuliang Liu, Biao Yang, Qiang Liu, Zhang Li, Zhiyin Ma, Shuo Zhang, and Xiang Bai. Textmonkey: An ocr-free large multimodal model for understanding document. *arXiv preprint arXiv:2403.04473*, 2024. 1, 2, 3, 4, 5, 7, 8
- [38] Ze Liu, Yutong Lin, Yue Cao, Han Hu, Yixuan Wei, Zheng Zhang, Stephen Lin, and Baining Guo. Swin transformer: Hierarchical vision transformer using shifted windows. In *Proceedings of the IEEE/CVF international conference on computer vision*, pages 10012–10022, 2021. 2, 5
- [39] Stuart Lloyd. Least squares quantization in pcm. *IEEE transactions on information theory*, 28(2):129–137, 1982. 2, 5
- [40] Ahmed Masry, Xuan Long Do, Jia Qing Tan, Shafiq Joty, and Enamul Hoque. Chartqa: A benchmark for question answering about charts with visual and logical reasoning. In *Findings of the Association for Computational Linguistics: ACL 2022*, pages 2263–2279, 2022. 6, 16
- [41] Minesh Mathew, Viraj Bagal, Rubèn Tito, Dimosthenis Karatzas, Ernest Valveny, and CV Jawahar. Infographicvqa. In *Proceedings of the IEEE/CVF Winter Conference on Applications of Computer Vision*, pages 1697–1706, 2022. 6, 16
- [42] Minesh Mathew, Dimosthenis Karatzas, and CV Jawahar. Docvqa: A dataset for vqa on document images. In *Proceedings of the IEEE/CVF winter conference on applications of computer vision*, pages 2200–2209, 2021. 6, 16
- [43] Nitesh Methani, Pritha Ganguly, Mitesh M Khapra, and Pratyush Kumar. Plotqa: Reasoning over scientific plots. In *Proceedings of the IEEE/CVF Winter Conference on Applications of Computer Vision*, pages 1527–1536, 2020. 6, 16
- [44] Anand Mishra, Shashank Shekhar, Ajeet Kumar Singh, and Anirban Chakraborty. Ocr-vqa: Visual question answering by reading text in images. In *2019 international conference on document analysis and recognition (ICDAR)*, pages 947–952. IEEE, 2019. 6

- [45] OpenAI. Chatgpt: Get answers. find inspiration. be more productive., 2022. Accessed: 2024-05-10. [1](#)
- [46] Panupong Pasupat and Percy Liang. Compositional semantic parsing on semi-structured tables. *arXiv preprint arXiv:1508.00305*, 2015. [6](#), [16](#)
- [47] Panupong Pasupat and Percy Liang. Compositional semantic parsing on semi-structured tables. *arXiv preprint arXiv:1508.00305*, 2015. [16](#)
- [48] Alec Radford, Jong Wook Kim, Chris Hallacy, Aditya Ramesh, Gabriel Goh, Sandhini Agarwal, Girish Sastry, Amanda Askell, Pamela Mishkin, Jack Clark, et al. Learning transferable visual models from natural language supervision. In *International conference on machine learning*, pages 8748–8763. PMLR, 2021. [5](#)
- [49] Yuzhang Shang, Mu Cai, Bingxin Xu, Yong Jae Lee, and Yan Yan. Llava-prumerge: Adaptive token reduction for efficient large multimodal models. *arXiv preprint arXiv:2403.15388*, 2024. [2](#), [7](#), [8](#)
- [50] Baoguang Shi, Cong Yao, Minghui Liao, Mingkun Yang, Pei Xu, Linyan Cui, Serge Belongie, Shijian Lu, and Xiang Bai. Icdar2017 competition on reading chinese text in the wild (rctw-17). In *2017 14th iapr international conference on document analysis and recognition (ICDAR)*, volume 1, pages 1429–1434. IEEE, 2017. [9](#)
- [51] Yongxin Shi, Dezhi Peng, Wenhui Liao, Zening Lin, Xinhong Chen, Chongyu Liu, Yuyi Zhang, and Lianwen Jin. Exploring ocr capabilities of gpt-4v (ision): A quantitative and in-depth evaluation. *arXiv preprint arXiv:2310.16809*, 2023. [2](#)
- [52] Štěpán Šimsa, Milan Šulc, Michal Uříčář, Yash Patel, Ahmed Hamdi, Matěj Kocián, Matyáš Skalický, Jiří Matas, Antoine Doucet, Mickaël Coustaty, et al. Docile benchmark for document information localization and extraction. In *International Conference on Document Analysis and Recognition*, pages 147–166. Springer, 2023. [6](#)
- [53] Amanpreet Singh, Vivek Natarajan, Meet Shah, Yu Jiang, Xinlei Chen, Dhruv Batra, Devi Parikh, and Marcus Rohrbach. Towards vqa models that can read. In *Proceedings of the IEEE/CVF conference on computer vision and pattern recognition*, pages 8317–8326, 2019. [9](#)
- [54] Tomasz Stanisławek, Filip Graliński, Anna Wróblewska, Dawid Lipiński, Agnieszka Kaliska, Paulina Rosalska, Bartosz Topolski, and Przemysław Biecek. Kleister: key information extraction datasets involving long documents with complex layouts. In *International Conference on Document Analysis and Recognition*, pages 564–579. Springer, 2021. [6](#)
- [55] AI Studio. Insurance text visual qa, 2022. [6](#)
- [56] Hongbin Sun, Zhanghui Kuang, Xiaoyu Yue, Chenhao Lin, and Wayne Zhang. Spatial dual-modality graph reasoning for key information extraction. *arXiv preprint arXiv:2103.14470*, 2021. [6](#)
- [57] S Svetlichnaya. Deepform: Understand structured documents at scale, 2020. [6](#), [16](#)
- [58] Ryota Tanaka, Taichi Iki, Kyosuke Nishida, Kuniko Saito, and Jun Suzuki. Instructdoc: A dataset for zero-shot generalization of visual document understanding with instructions. *arXiv preprint arXiv:2401.13313*, 2024. [2](#), [3](#)
- [59] Ryota Tanaka, Kyosuke Nishida, and Sen Yoshida. Visualmrc: Machine reading comprehension on document images. In *Proceedings of the AAAI Conference on Artificial Intelligence*, volume 35, pages 13878–13888, 2021. [6](#), [16](#)
- [60] Jingqun Tang, Chunhui Lin, Zhen Zhao, Shu Wei, Binghong Wu, Qi Liu, Hao Feng, Yang Li, Siqi Wang, Lei Liao, et al. Textsquare: Scaling up text-centric visual instruction tuning. *arXiv preprint arXiv:2404.12803*, 2024. [2](#)
- [61] Jingqun Tang, Qi Liu, Yongjie Ye, Jinghui Lu, Shu Wei, Chunhui Lin, Wanqing Li, Mohamad Fitri Faiz Bin Mahmood, Hao Feng, Zhen Zhao, et al. Mtvqa: Benchmarking multilingual text-centric visual question answering. *arXiv preprint arXiv:2405.11985*, 2024. [2](#)

- [62] InternLM Team. Internlm: A multilingual language model with progressively enhanced capabilities, 2023. [1](#)
- [63] The Vicuna Team. Vicuna: An open-source chatbot impressing gpt-4 with 90 Accessed: 2024-05-10. [1](#)
- [64] Tianchi. Ocr text reading order sorting dataset, 2020. [6](#)
- [65] Hugo Touvron, Thibaut Lavril, Gautier Izacard, Xavier Martinet, Marie-Anne Lachaux, Timothée Lacroix, Baptiste Rozière, Naman Goyal, Eric Hambro, Faisal Azhar, et al. Llama: Open and efficient foundation language models. *arXiv preprint arXiv:2302.13971*, 2023. [1](#)
- [66] Michał Turski, Tomasz Stanisławek, Karol Kaczmarek, Paweł Dyda, and Filip Graliński. Ccpdf: Building a high quality corpus for visually rich documents from web crawl data. In *International Conference on Document Analysis and Recognition*, pages 348–365. Springer, 2023. [6](#)
- [67] Ramakrishna Vedantam, C Lawrence Zitnick, and Devi Parikh. Cider: Consensus-based image description evaluation. In *Proceedings of the IEEE conference on computer vision and pattern recognition*, pages 4566–4575, 2015. [16](#)
- [68] Andreas Veit, Tomas Matera, Lukas Neumann, Jiri Matas, and Serge Belongie. Coco-text: Dataset and benchmark for text detection and recognition in natural images. *arXiv preprint arXiv:1601.07140*, 2016. [9](#)
- [69] Yonghui Wang, Wengang Zhou, Hao Feng, Keyi Zhou, and Houqiang Li. Towards improving document understanding: An exploration on text-grounding via mllms. *arXiv preprint arXiv:2311.13194*, 2023. [2](#)
- [70] Haoran Wei, Lingyu Kong, Jinyue Chen, Liang Zhao, Zheng Ge, Jinrong Yang, Jianjian Sun, Chunrui Han, and Xiangyu Zhang. Vary: Scaling up the vision vocabulary for large vision-language models. *arXiv preprint arXiv:2312.06109*, 2023. [1](#), [2](#), [3](#), [7](#), [9](#)
- [71] Siyuan Wei, Tianzhu Ye, Shen Zhang, Yao Tang, and Jiajun Liang. Joint token pruning and squeezing towards more aggressive compression of vision transformers. In *Proceedings of the IEEE/CVF Conference on Computer Vision and Pattern Recognition*, pages 2092–2101, 2023. [5](#)
- [72] Siyuan Wei, Tianzhu Ye, Shen Zhang, Yao Tang, and Jiajun Liang. Hrvda: High-resolution visual document assistant. In *Proceedings of the IEEE/CVF Conference on Computer Vision and Pattern Recognition*, 2024. [1](#), [2](#), [3](#), [7](#)
- [73] Aiyuan Yang, Bin Xiao, Bingning Wang, Borong Zhang, Ce Bian, Chao Yin, Chenxu Lv, Da Pan, Dian Wang, Dong Yan, et al. Baichuan 2: Open large-scale language models. *arXiv preprint arXiv:2309.10305*, 2023. [1](#)
- [74] Jiabo Ye, Anwen Hu, Haiyang Xu, Qinghao Ye, Ming Yan, Guohai Xu, Chenliang Li, Junfeng Tian, Qi Qian, Ji Zhang, et al. Ureader: Universal ocr-free visually-situated language understanding with multimodal large language model. *arXiv preprint arXiv:2310.05126*, 2023. [1](#), [2](#), [3](#), [4](#), [7](#)
- [75] Qinghao Ye, Haiyang Xu, Guohai Xu, Jiabo Ye, Ming Yan, Yiyang Zhou, Junyang Wang, Anwen Hu, Pengcheng Shi, Yaya Shi, et al. mplug-owl: Modularization empowers large language models with multimodality. *arXiv preprint arXiv:2304.14178*, 2023. [7](#)
- [76] Ya-Qi Yu, Minghui Liao, Jihao Wu, Yongxin Liao, Xiaoyu Zheng, and Wei Zeng. Texthawk: Exploring efficient fine-grained perception of multimodal large language models. *arXiv preprint arXiv:2404.09204*, 2024. [1](#), [2](#), [4](#), [7](#)
- [77] Hesuo Zhang, Lingyu Liang, and Lianwen Jin. Scut-hccdoc: A new benchmark dataset of handwritten chinese text in unconstrained camera-captured documents. *Pattern Recognition*, 108:107559, 2020. [6](#)
- [78] Shuo Zhang, Biao Yang, Zhang Li, Zhiyin Ma, Yuliang Liu, and Xiang Bai. Exploring the capabilities of large multimodal models on dense text. *arXiv preprint arXiv:2405.06706*, 2024. [1](#), [7](#), [8](#), [9](#)

- [79] Xu Zhong, Elaheh ShafieiBavani, and Antonio Jimeno Yepes. Image-based table recognition: data, model, and evaluation. In *European conference on computer vision*, pages 564–580. Springer, 2020. 6
- [80] Fengbin Zhu, Wenqiang Lei, Youcheng Huang, Chao Wang, Shuo Zhang, Jiancheng Lv, Fuli Feng, and Tat-Seng Chua. Tat-qa: A question answering benchmark on a hybrid of tabular and textual content in finance. *arXiv preprint arXiv:2105.07624*, 2021. 6

Appendix

A Benchmark Datasets Evaluation Metrics

DocVQA [42], InfoVQA [41], ChartQA [40], WTQ [47], and VisualMRC [59] are all datasets designed for visual document image question answering. DocVQA encompasses a variety of document types, featuring a rich diversity of questions and data types. InfoVQA focuses on infographics that contain an abundance of visual elements. ChartQA and WTQ specifically target question answering for chart data and tabular data, respectively. VisualMRC, on the other hand, places a greater emphasis on developing natural language understanding and generation capabilities. DeepForm [57], FUNSD [19], SROIE [18], and POIE [25] are key information extraction datasets where the model is required to identify the value corresponding to a given key.

Widely used text-centric benchmarks employ diverse metrics to better capture the distinct characteristics among various datasets. As depicted in Table 4 within the main text, both DocVQA [42] and InfoVQA [41] utilize ANLS [4] as their metric. The results reported are evaluated on their respective official websites. ChartQA [40] is evaluated by accuracy relaxed accuracy [43], while VisualMRC [59] relies on CIDEr [67]. DeepForm [57] is measured by F1 score, and WTQ [46] evaluated by accuracy.

B More Details and Results of Adaptive Pixel Slimming

Algorithm 2 Adaptive Pixel Slimming

Require:

Source document image $I_S \in \mathbb{R}^{H \times W \times 3}$
SIZE=2048
 $t_n = 50$
 $t_c = 10$
ICR(Identify continuous regions where the values exceed t_v and the count of consecutive occurrences is greater than t_c)
1: Sobel $_x$ = abs(Sobel(I_S , direction= x))
2: Sobel $_y$ = abs(Sobel(I_S , direction= y))
3: Initialize $I_G \in \mathbb{R}^{H \times W}$
4: $I_G(i, j) = \max(\text{Sobel}_x(i, j), \text{Sobel}_y(i, j))$
5: $I_G[I_G < t_n] = 0$
6: $I_G = \text{resize}(I_G, (\text{SIZE}, \text{SIZE}))$
7: $\text{sum}_y = \text{sum}(I_G(i, j), \text{along } y \text{ direction}) \in \mathbb{R}^{\text{SIZE}}$
8: $\text{blocks}_y = \text{ICR}(\text{sum}_y, t_v, t_c)$
9: $\text{blocks}_y = \text{normalize_to_original_size}(\text{blocks}_y, (H, W), \text{SIZE})$
10: $\text{sum}_x = \text{sum}(I_G(i, j), \text{along } x \text{ direction}) \in \mathbb{R}^{\text{SIZE}}$
11: $\text{blocks}_x = \text{ICR}(\text{sum}_x, t_v, t_c)$
12: $\text{blocks}_x = \text{normalize_to_original_size}(\text{blocks}_x, (H, W), \text{SIZE})$
13: $I_t = \text{remove_blocks}(\text{blocks}_y, \text{blocks}_x, I_S)$
14: **return** I_t

The specific computation method and parameter settings for Adaptive Pixel Slimming are detailed in Algorithm 2, which provides additional details beyond the main text: 1. The 2D gradient map is obtained by taking the maximum value from the gradient maps in the x and y directions. This approach aims to ensure the accuracy of redundancy detection while minimizing false positives. Using the maximum value rather than the average prevents the removal of regions with features in a single direction, such as table lines. 2. Noise removal is performed by setting gradient values below a threshold t_n to zero, thereby reducing interference from background texture noise. 3. Before identifying redundant regions based on the value threshold t_v , we normalize the gradient map to a fixed resolution. This normalization ensures that the threshold is robust to varying resolutions.

In Fig. 6, we present some results of Adaptive Pixel Slimming, demonstrating its effectiveness in removing redundant regions from document images and reducing image resolution. The impact on natural scene images is minimal.

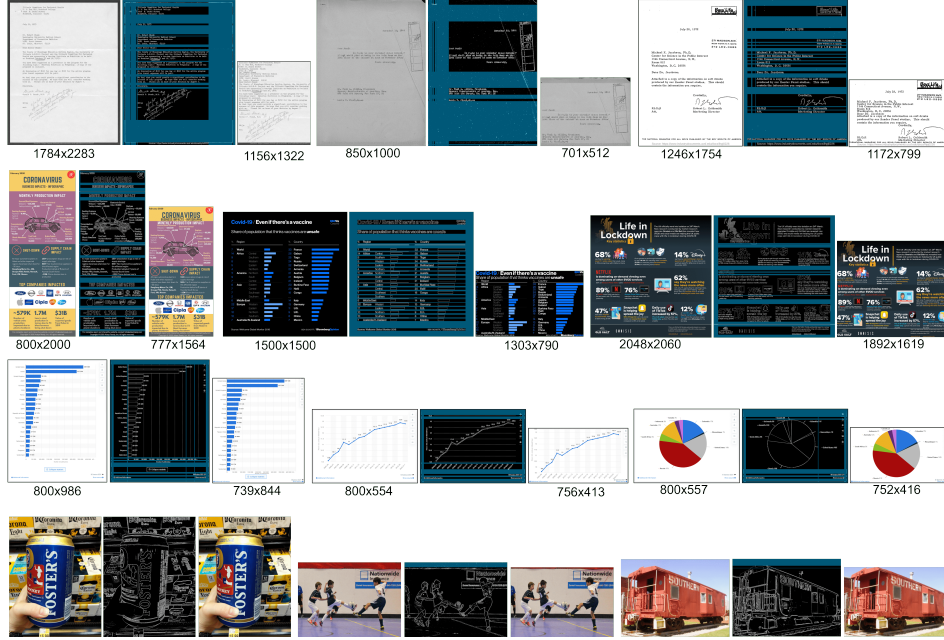


Figure 6: Additional visual results of Adaptive Pixel Slimming on various types of data. The redundant regions identified by Adaptive Pixel Slimming are highlighted on the corresponding gradient maps. The resolution for some images is indicated below the respective images.

C More Details of DTS

Algorithm 3 Similarity Weighted Aggregation

Require:

```

essential_tokens
nonessential_tokens
FMS (find the most similar token)
1: mappings = { }
2: for token in nonessential_tokens:
3:   most_similar_essential_token = FMS(token, tokens in essential_tokens )
4:   mappings[token] = most_similar_essential_token
5: updated_essential_tokens = []
6: for token in essential_tokens:
7:   similar_nonessential_tokens = []
8:   for key,value in mappings:
9:     if token == value:
10:      similar_nonessential_tokens.append(key)
11: if len(similar_nonessential_tokens)==0:
12:   updated_essential_tokens.append(token)
13: else:
14:   updated_essential_tokens.append(weighted_sum(token, similar_nonessential_tokens))
15: return updated_essential_tokens

```

D Declaration of Potential Harmful Content

While our model performs well on many tasks, we acknowledge that, like all MLLMs, due to the breadth of its training data and the diversity of its content, our model may occasionally generate inaccurate, misleading, or harmful content.

We hereby declare that, despite our efforts to mitigate this risk by selecting appropriate training data and adjusting model parameters, we cannot entirely eliminate the possibility of the MLLM producing harmful content. Therefore, when referring to this paper or using the model proposed herein, please

be aware that the generated text may contain uncertainties and risks. We encourage readers to exercise caution and independently assess the accuracy and credibility of the content generated by the MLLM.